Nontrivial Redox Behavior of Nanosized Cobalt: New Insights from Ambient Pressure X-ray Photoelectron and Absorption Spectroscopies

Vasiliki Papaefthimiou,[†] Thierry Dintzer,[†] Véronique Dupuis,[‡] Alexandre Tamion,[‡] Florent Tournus,[‡] Arnaud Hillion,[‡] Detre Teschner,[§] Michael Hävecker,[§] Axel Knop-Gericke,[§] Robert Schlögl,[§] and Spyridon Zafeiratos[†,*]

[†]Laboratoire LMSPC UMR7515, CNRS, University of Strasbourg, F-67087, Strasbourg cedex 2, France, [‡]Laboratoire PMCN UMR 5586, University of Lyon 1, CNRS, F-69622, Villeurbanne cedex, France, and [§]Fritz-Haber-Institut der Max-Planck-Gesellschaft, Faradayweg 4-6, 14195 Berlin, Germany

ABSTRACT The reduction and oxidation of carbon-supported cobalt nanoparticles (3.50 ± 0.22 nm) and a Co (0001) single crystal was investigated by ambient pressure X-ray photoelectron (APPES) and X-ray absorption (XAS) spectroscopies, applied *in situ* under 0.2 mbar hydrogen or oxygen atmospheres and at temperatures up to 620 K. It was found that cobalt nanoparticles are readily oxidized to a distinct CoO phase, which is significantly more stable to further oxidation or reduction compared to the thick oxide films formed on the Co(0001) crystal. The *nontrivial* size-dependence of redox behavior is followed by a difference in the electronic structure as suggested by theoretical simulations of the Co L−edge absorption spectra. In particular, contrary to the stable rocksalt and spinel phases that exist in the bulk oxides, cobalt nanoparticles contain a significant portion of metastable wurtzite-type CoO.

KEYWORDS: cobalt · nanoparticles · wurtzite CoO · redox properties · XPS · APPES · NEXAFS

Cobalt and its oxides are critical components in many technological areas including spintronics,[1,2] Li-ion batteries,[3] and catalytic Fischer−Tropsch synthesis (FTS).[4] The reduction/oxidation (redox) properties of cobalt are closely related to the stability and performance of the cobalt-based applications. For example, if cobalt is not completely reduced, its catalytic performance during FTS decreases.[4] Nanometer-sized cobalt particles (Co NPs) might deviate from bulk-like behavior due to the large fraction of atoms at their surface and the finite number of atoms within each particle. It has been reported that cobalt crystallites with sizes below 5−6 nm are rapidly oxidized and deactivated under realistic FTS conditions.[5] In addition, the surface specific activity (turnover frequency, TOF) of FTS reaction is significantly decreased when the cobalt particle size is below 10 nm[6] or, according to another group, 5 nm.[7−9]

Bulk cobalt oxide typically crystallizes into two stable structures; the CoO rocksalt structure with octahedral Co^{2+} and the Co_3O_4 spinel structure with octahedral Co^{3+} and tetrahedral Co^{2+} cations. A few years ago, synthesis of a new pure form of CoO, the hexagonal wurtzite CoO with tetrahedral Co^{2+} cations, was reported by two groups.[10−12] Moreover, wurtzite-CoO can be stabilized in Co-doped ZnO solid solution ($Zn_{1-x}Co_xO$).[13] Recently it was found that CoO films of nanosized thickness should not be considered as a crystallographically pure phase; though the innerside of the nanosized films is of a rocksalt structure, they are terminated (in the top four layers) by a thin slab of wurtzite-type CoO.[14] Finally, the existence of the wurtzite structure was also claimed for thicker films.[15]

Early surface science studies probing oxidation of single crystalline and polycrystalline cobalt surfaces exposed to molecular oxygen in high vacuum conditions[16−19] indicated that the primary step of surface oxidation is the accumulation of chemisorbed oxygen, which can readily take place even at 120 K. As a next step, the surface adsorbed oxygen diffuses in the inner Co layers, leading to the formation of surface oxide. This process critically depends on the temperature and the availability of oxygen in the gas phase. At subambient temperatures Co_3O_4 oxide is directly formed, while at room temperature the initially formed CoO oxide is further oxidized to Co_3O_4 at higher oxygen exposures (two-step processes).

* Address correspondence to spiros.zafeiratos@unistra.fr.

Received for review December 9, 2010 and accepted January 25, 2011.

Published online February 10, 2011
10.1021/nn103392x

However in all cases the final oxidation product is the spinel Co_3O_4. Apart from the UHV-based studies, the redox chemistry of cobalt has been investigated at high temperature−pressure regime by many techniques.[20−22] Although these studies provided valuable information on the cobalt oxidation mechanism (*i.e.*, the growth and the oxidation kinetics), the surface state of Co oxides was not determined since surface sensitive techniques could not be applied at such conditions. Recently, Salmeron and co-workers showed by using X-ray absorption spectroscopy, that oxidized Co NPs with sizes between 3 and 10 nm supported on a Au foil could be readily reduced in 1 bar of hydrogen at 600 K.[6] They also found that smaller NPs were easier to reduce than the larger ones, which is the opposite behavior to what was previously known for oxide-supported cobalt NPs.[4]

Ex situ studies of cobalt redox chemistry can give inadequate results because the cobalt surface state can easily change by exposure to air. This limitation is particularly important when studying nanosized samples. In the present report a combination of ambient pressure photoelectron (APPES) and X-ray absorption spectroscopies (XAS) was applied *in situ* to clarify the surface reactivity of Co NPs and Co(0001) single crystal toward O_2 and H_2 atmospheres in the mbar pressure regime and at elevated temperatures. Moreover, a theoretical simulation of XAS spectra using the charge transfer multiplet (CTM) approach allowed reporting on the electronic structure of the oxides. Significant differences were observed in the redox properties of NPs and bulk cobalt, which are related to the size-dependent electronic structure of cobalt oxide.

RESULTS AND DISCUSSION

Stability of Co NPs. Although the sample preparation method assures small and almost monodisperse cobalt nanoparticles size, coalescence due to thermal annealing and gas exposure might influence their actual size in the course of the experiment.[23] To estimate the degree of particle agglomeration upon annealing in gas atmospheres, the intensity ratio of the Co2p (nanoparticles) and C1s (mainly due to the amorphous carbon substrate) core level peaks measured at the same photoelectron kinetic energy (580 eV), was monitored *in situ* as a function of the annealing temperature and is shown in Figure 1b. The Co2p/C1s intensity ratio is directly related to cobalt dispersion on the support. In the case of agglomeration less cobalt and more carbon surface is exposed; therefore, lower Co2p/C1s ratios are expected. Figure 1b indicates that the relative Co2p/C1s intensity ratio, referring to the freshly prepared sample, decreases by about 20% upon annealing at the maximum temperature studied here (620 K). To estimate the equivalent mean particle size increase, a simple quantitative model was applied to fit the experimental data. For the calculations cobalt

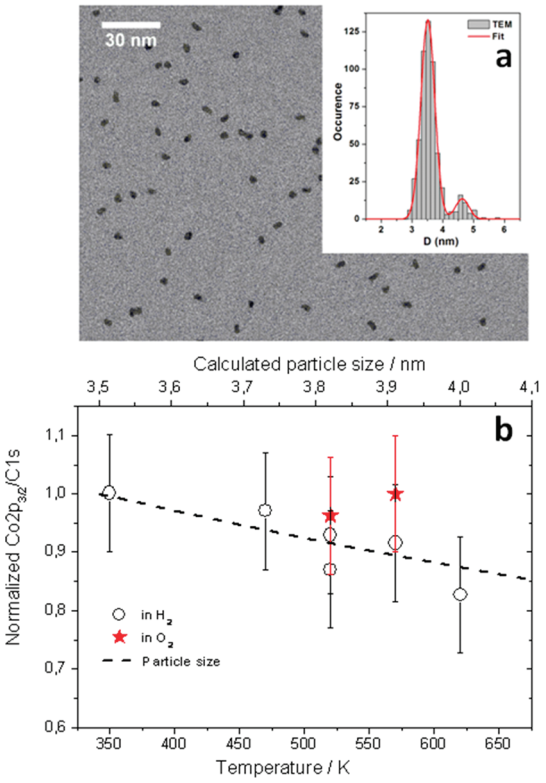

Figure 1. (a) TEM image of Co clusters and the histogram of the corresponding size distribution (top right corner), (b) The evolution of $Co2p_{3/2}$ to C 1s intensity ratio derived by APPES measurements as a function of the annealing temperature in 0.2 mbar H_2 (open circles) and O_2 (stars) atmospheres. The error bar in the intensity ratio is estimated ±10%. The dashed line corresponds to the calculated particle size evolution, using a cubic particle shape model.

particles were described by a geometric cubic shaped model with initial cube edge of 3.5 nm and Co NPs density of 2×10^{11} NPs·cm^{-2} (estimated from TEM image analysis). We note that the cubic shape is an approximation used to facilitate the calculations and does not represent the physical shape of the nanoparticles, which is most likely a truncated octahedron. The good resemblance of the calculated and experimental values indicates that the mean Co particle size does not exceed 4 nm even after heating at 620 K. Therefore no significant Co particle reorganization occurs under our experimental conditions, in agreement with previous TEM studies on supported Co NPs.[23] In order to ensure that Co NPs coalescence will remain at low levels, the sample was never annealed at temperatures higher than 620 K.

Oxidation of Cobalt. Cobalt oxidation in 0.2 mbar O_2 was studied at 520 and 570 K. The $Co2p_{3/2}$ photoemission and Co $L_{3,2}$ absorption spectra of Co NPs and Co(0001) crystal are summarized in Figure 2 panels a and b, respectively. In both cases the $Co2p_{3/2}$ peak consists of a sharp main component and a satellite feature at the high binding energy side. For the Co-(0001) crystal at 520 K, the main $Co2p_{3/2}$ peak at 779.6 eV with a broad-weak satellite at 788.5 eV (lower spectrum,

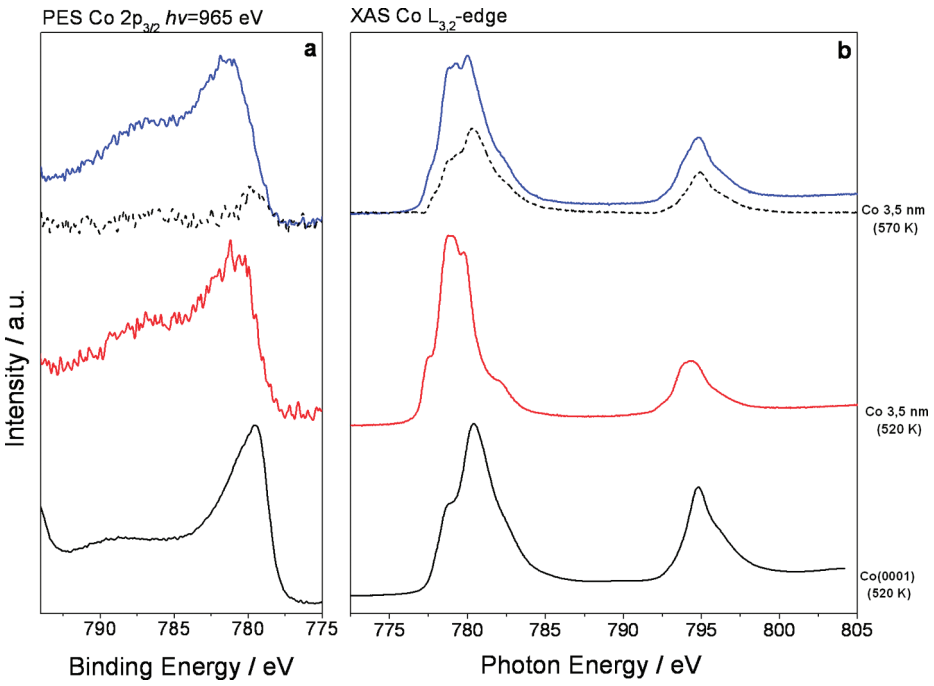

Figure 2. (a) Co2p$_{3/2}$ photoemission and (b) Co L$_{3,2}$ absorption edge of Co(0001) crystal at 520 K (bottom spectra) and 3.5 nm Co NPs (middle and top spectra) at 520 K/570 K under 0.2 mbar O_2. Dashed lines are the difference spectrum between 520 and 570 K.

Figure 2a) is characteristic of spinel bulk-like Co_3O_4.[24] In addition, the corresponding Co L$_{3,2}$ absorption edge (lower spectrum, Figure 2b) is also in good agreement with previous published XAS results from Co_3O_4 compounds.[25,26] Therefore, one can safely point to a thick (>5 nm) bulk-like Co_3O_4 layer formation on the Co(0001) surface.

For NPs, the Co2p$_{3/2}$ peak recorded at 520 K (middle spectrum, Figure 2a) is shifted at higher binding energies by ca. 1 eV compared to the bulk, while the intensity of its satellite structure is significantly enhanced. Interpretation of the photoemission results based on absolute binding energies might be misleading, especially when dealing with nanosized oxides, due to charging and/or size effects related to photoionization.[27] Therefore we focus on the intensity and the relative position of the satellite peak. Modifications of the Co 2p satellite have been directly related to the oxide stoichiometry and are extremely sensitive to cobalt oxidation state.[24,27,28] The intense satellite structure is a clear indication of Co^{2+} cations with partially filled e_g character like in the octahedrally coordinated bulk CoO.[27] The Co L$_{3,2}$ edge absorption spectrum of NPs is also notably different compared to bulk-like Co_3O_4 as is evident in Figure 2b. The fine structure of the Co NPs absorption edge is characteristic of octahedrally coordinated Co^{2+} species of CoO-type,[26] in line with the photoemission results. Further annealing of Co NPs at 570 K modifies the Co 2p peak (upper spectra of Figure 2). In particular, the Co 2p$_{3/2}$ photoemission peak is shifted about 1.5 eV toward higher energies as compared to the bulk Co, while its satellite intensity is slightly enhanced. Additionally, in the Co L$_{3,2}$ absorption edge the features around 778 and 781 eV are significantly different. To obtain a better description of the Co 2p and L-edge modifications induced upon annealing at 570 K, the spectra at 520 K were subtracted from those at 570 K. As shown, the difference curves for both photoemission and absorption spectra (dash lines) resemble very much those of bulk-like Co_3O_4. Therefore, it is reasonable to assume that at 570 K Co NPs are oxidized to a CoO/Co_3O_4 mixture. Keeping in mind that in both oxides the O^{2-} ions arrange in fcc lattice structure,[24] one can envision that the CoO/Co_3O_4 mixture consists of a common oxygen sublattice with local variation of Co^{2+} and Co^{3+} cations occupying the octahedral and tetrahedral sites. Although the kinetics of cobalt NPs oxidation was not analyzed in detail, we note that XAS spectra recorded in different exposure durations (see Supporting Information S1) were almost identical, indicating that NPs oxidation is primarily a thermodynamically driven process that results in the stabilization of the NPs. To conclude, upon annealing bulk Co single crystal and Co NPs under 0.2 mbar O_2 the formation of Co_3O_4 is favored on the bulk Co. The 3.5 nm Co NPs are readily oxidized to a CoO-type oxide, but total oxidation to Co_3O_4 is not favored even after annealing at higher temperatures than that of the bulk Co sample.

Reduction of Cobalt. The reduction of cobalt was studied by exposing the preoxidized samples (see Figure 2) in 0.2 mbar H_2 at room temperature and progressively annealing up to 620 K. The photoemission and absorption spectra for NPs and bulk Co are

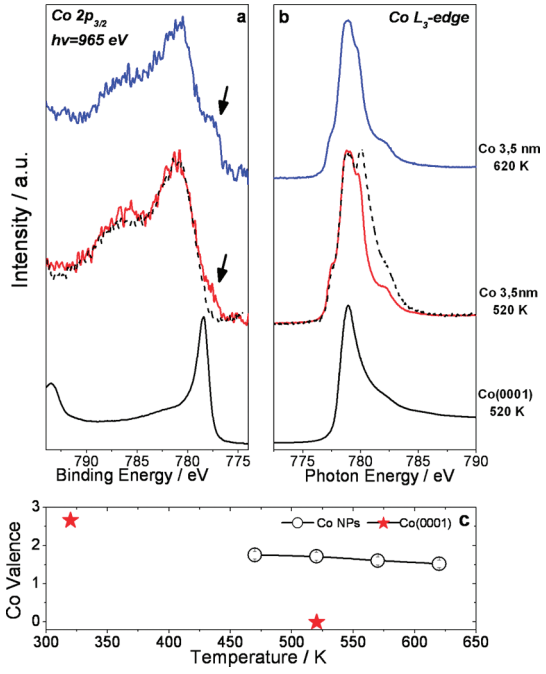

Figure 3. (a) Co2p$_{3/2}$ photoemission and (b) Co L$_3$ absorption edge of Co(0001) crystal at 520 K (bottom spectra) and 3.5 nm Co NPs (middle and top spectra) at 520 K/620 K under 0.2 mbar H_2. The spectra obtained prior to the reduction treatment are presented as dash lines. Evolution of new species during reduction is indicated by the arrow. (c) The average cobalt valence for the bulk-like (stars) and nano (open circles) cobalt oxides as a function of the annealing temperature.

presented in Figure 3 panels a and b, respectively. The Co_3O_4 layer formed on the surface of bulk-Co is readily reduced to the metallic state after annealing at 520 K, as is evident by the characteristic Co 2p$_{3/2}$ and L$_3$ lines (bottom spectra, Figure 3a,b).[29] In the case of oxidized Co NPs, the Co_3O_4 contribution to the Co L$_3$-edge disappears, but NPs remain oxidized to a CoO-type oxide as indicated by the shape of the absorption edge shown in Figure 3b (middle spectrum). In the Co 2p$_{3/2}$ peak, apart from the CoO characteristic intense satellite structure, a new component at lower binding energy (indicated by an arrow) is observed referring to the spectrum recorded in O_2 (dash line). The new component is due to reduced/metallic state cobalt species (Co_{met}), typically found between 1.3 and 2.3 eV lower than Co^{2+} in cobalt oxides.[30] Upon annealing at 620 K, Co_{met} intensity increases, however the majority of the Co NPs remain oxidized. Since metallic and oxide cobalt components are well separated in the Co 2p$_{3/2}$ region, a linear combination of reference spectra was used to calculate the Co average valence at each temperature (Figure 3c). For comparison, data recorded on the oxidized Co(0001) surface under the same conditions are included in the graph. As is evident from Figure 3c, the bulk-like cobalt oxide is fully reduced to the metallic state at 520 K, while the oxide formed on NPs is only partially reduced even at 620 K. Due to the overlapping between metallic and oxide Co L$_3$-edges their contribution in the absorption spectrum cannot unequivocally resolved, nevertheless the shape of the Co L$_3$-edge seems to modify as Co NPs are reducing. To obtain more insight on the electronic state of cobalt after reduction, a reference spectrum of metallic Co was subtracted from the Co L-edge recorded at 620 K in H_2 (see Supporting Information S2). The resulting curve, corresponding to the remaining oxide species after reduction, is slightly different from the spectrum at 520 K in O_2 (under these condition Co NPs form a CoO-type oxide). In particular the shoulder at 777 eV is less intense in the difference spectrum, while the peaks at 779−780 eV are slightly higher (see Supporting Information S2). The reason of these differences is probably variations in the electronic structure of cobalt oxide remaining after reduction, the implications of this observation will be discussed in the next paragraphs.

The morphology of the oxidized CoO NPs might be critical for their stability; that is, the core−shell structure is reported to be more stable than the agglomerated non- core−shell one.[31] To probe if there is a layered structure of Co_{met} and CoO in the particles, or the two phases are randomly mixed, depth-depended measurements were performed. The Co 2p$_{3/2}$ peak was recorded by using four different photon energies, thus four information depths. It was found (see Supporting Information S3) that the metallic cobalt intensity slightly increases at higher photon energies. This is probably due to core−shell structure with Co_{met} species encapsulated under CoO, in agreement with previously published results.[26,32] Notably the cobalt oxidation state could only be observed by *in situ* measurements. Modifying the sample conditions (temperature, gas environment, *etc.*) had a direct effect on its surface state (Supporting Information S4), highlighting the importance of tracking the surface structure by *in situ* methods. Therefore post-mortem analysis of the samples by other techniques, for example using microscopy, might lead to erroneous interpretations, and only *in situ* techniques, like environmental TEM, could be used to confirm the cobalt oxide structures.

The Electronic Structure of "Nano-CoO". The above presented results showed that Co NPs are readily oxidized to a CoO-type oxide (denoted for brevity as "nano-CoO"). However, unlike observations on bulk-like CoO, the nano-CoO is resistant to both further oxidation to Co_3O_4, and to reduction to metallic cobalt under the conditions applied here. The difficulty to reduce preoxidized Co NPs, compared to larger particles, has been previously observed for cobalt supported on oxides.[25,26,33] This behavior has been attributed to strong cobalt-support interaction effects which stabilizes the small particles by forming irreducible mixed oxides, like cobalt aluminates or silicates. On the contrary, carbon is considered as a chemically inert support[4,7] and has been previously used to study the

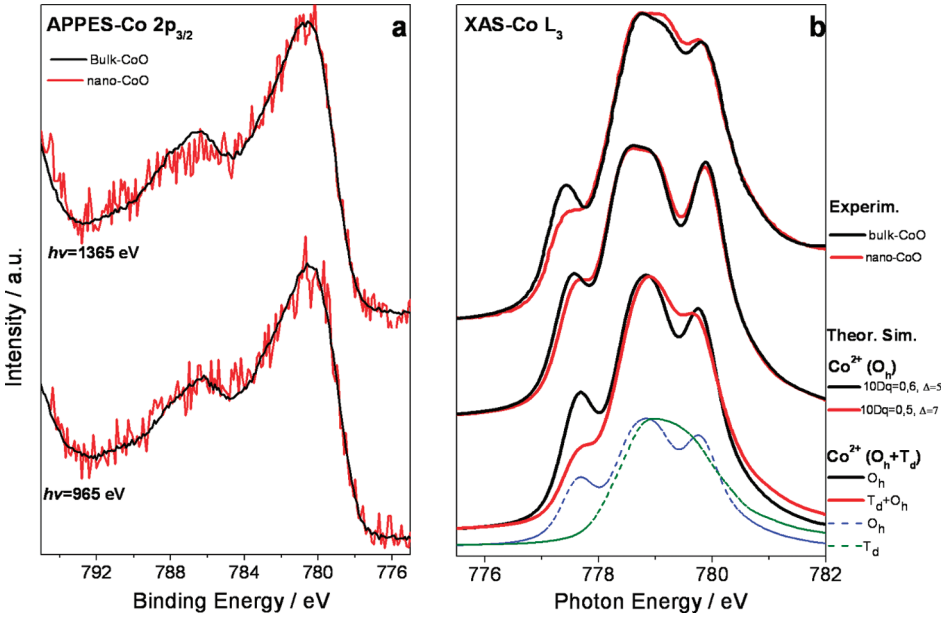

Figure 4. (a)The Co $2p_{3/2}$ photoelectron peak of bulk (black line) and nano CoO (red line) recorded at 520 K using 1365 (top) and 965 eV (bottom) photon energies. For comparison the spectra have been normalized to the same height and shifted to the same binding energy. (b) The experimental (top) and theoretically simulated (middle and bottom) Co L_3-edge absorption spectra for nano and bulk CoO. The experimental curves are recorded at 520 K. The middle spectra correspond to the best possible simulation assuming octahedrally coordinated (O_h symmetry) Co^{2+} cations. The bottom spectra are linear combination of theoretical curves[26] of octahedral and tetrahedral (T_d) Co^{2+} cations in two compositions.

intrinsic activity of cobalt particles.[7,8] To rationalize this observation, more insights to the cobalt electronic structure are given.

In Figure 4a we compare the Co $2p_{3/2}$ photoemission spectra of CoO-type oxides formed on NPs and Co(0001) crystal[34] recorded by two different photon energies at 520 K. The photoemission spectra of both samples are similar, and neither Co_{met} nor Co_3O_4 species are present in a large extent. A subtle decrease of the nano-CoO Co 2p satellite intensity obtained using 1365 eV photon energy, might indicate defects and minor compositional variations from the CoO stoichiometry. The intensity and energy position of the satellite peak, which is sensitive to the ionic environment around cobalt, suggests that both oxides mainly consist of high spin Co^{2+} cations.[24] However, Co^{2+} cations are not necessarily coordinated with the same symmetry in the two cases, since Co^{2+} in octahedral and tetrahedral environment exhibit very similar satellite peaks in the Co 2p photoemission spectrum.[27] On the contrary, the symmetry of Co^{2+} cations has a pronounced effect on the shape of the absorption edge, with octahedrally and tetrahedrally coordinated Co^{2+} ions having very different Co $L_{3,2}$-edge characteristics.[26] A closer look in the experimental L_3-edge lines (upper spectra, Figure 4b), indicates that the intensity of the peak at ~777 eV is significantly declined for nano-CoO followed by a slight increase at the 779 eV area. Simulation of the Co L_3-edge using multiplet calculations (*CTM4XAS*) is included in Figure 4b to support the interpretation of the experimental data. The calculations were performed in two ways: in one scheme we assumed that Co ions are arranged in octahedral symmetry (like in the bulk CoO), while in the other a linear combination of individually calculated octahedral and tetrahedral high spin Co^{2+} was used to simulate the experimental results.

The two key parameters affecting the shape of the calculated XAS curves are 10*Dq* (crystal field splitting) and Δ (charge transfer energy). It should be noted that these parameters are determined by comparison between simulated and experimentally derived spectra and not by *ab initio* calculations. The 10*Dq* value corresponds to the one-electron energy difference between the t_{2g} and e_g Co 3d orbitals in an octahedral crystal field at the ground state. It is related to cooperative structural effects[35,36] and depends on the metal−ligand distance, *R*, in a way that an increase in the value of 10*Dq* corresponds to a decrease in Co−O distance.[37,38] The charge transfer energy term Δ describes the interaction of Co^{2+} ions with delocalized electrons from the O 2p orbital. An increase in Δ value corresponds to an increase in the $3d^8$ to $3d^9L$ ratio in the ground state; that is, the Co 3d -state interacts less with O 2p orbitals. The simulation of our bulk-like CoO spectrum using parameters close to those previously reported in the literature gave quite satisfactory results. An increase of Δ (7 instead of 3) compared to the literature values for bulk CoO[26] might be induced by less interacting Co and O ions in the CoO thick film formed on Co(0001) compared to the bulk CoO. Despite an extensive variation of input parameters, the intensity drop of the 777 eV peak observed in nano-CoO could not be satisfactorily reproduced in the

octahedral model. In the best case, for lower 10*Dq* and higher Δ values, the component at 777 eV is slightly decreasing while it is shifted closer to the peak at 780 eV (middle curves of Figure 4b). The decrease of 10*Dq* and increase of Δ values is an indication of larger Co−O distances and less Co−O interaction for nano-CoO compared the bulk. On the basis of these results one can propose a modified crystal structure of nano-CoO. In particular, since in nano-CoO the Co−O bond is expected to be less ionic, tetrahedral coordination of Co^{2+} ions is favored, in contrast to the octahedral, more ionic, bulk Co−O bonds.[39]

Accordingly, to describe the L_3-edge differences in a more sophisticated approach, mixed octahedral (O_h) and tetrahedral (T_d) Co^{2+} ion coordination was considered, using charge transfer parameters proposed by Morales *et al*. for bulk cobalt oxides.[26] In the bottom spectrum of Figure 4b the theoretical curves of Co^{2+} (O_h) and linear combinations of Co^{2+} (O_h) and Co^{2+} (T_d) with ratio 1:1 are compared. As is evident, the simulated peak using 1:1 ratio resembles very much the drop of the feature at 777 eV found for nano-CoO. Even the slight increase in intensity around 779 eV, shown in the experimental curves, is satisfactorily reproduced. Therefore, on the basis of the mixed site coordination model, the differences in the XAS spectra of bulk and nano-CoO could be qualitatively understood by a conjunction of the two oxide geometries, indicating that nano-CoO is most probably a mixed structural phase of wutzite- and rocksalt-type CoO, (denoted for brevity as w-CoO and r-CoO, respectively).

General Discussion. The above presented results clearly show that the redox behavior of nanometer scale cobalt is drastically different compared to its bulk counterpart. This is though not surprising, since the unique chemical properties of low-dimensional oxide nanostructures are already well established.[40] It was however interesting to find that Co NPs do not follow the expected route of fast oxidation and reduction, underlined by the fast kinetics of their limited size, but show the reverse trend. Next, we attempt to rationalize the "*non-classical*" size effect of cobalt redox behavior.

Analysis of our XAS results indicates the existence of w-CoO in NPs but not in the bulk material. The driving force of stabilizing the metastable w-CoO on the nanoparticles is not yet fully understood. Finite-size effects may induce extra pressure to the NPs due to surface tension, inhibiting phase transformations. This is well documented for metallic cobalt, where enhanced surface tension may inhibit the fcc-to-hcp phase transformation at room temperature for nano-sized but not for bulk cobalt.[41] Furthermore, the smaller the size of the NPs the more influential the support effect is expected. On oxide supports, formation of irreducible mixed oxides has been suggested as a deactivation mechanism of small Co NPs.[4] Of course our amorphous carbon support is chemically inert to oxide formation, but might actively participate to the stabilization of Co NPs either by causing epitaxial strain to the supported NPs or by cobalt carbide formation. Defects pre-existing on the amorphous carbon support might anchor Co NPs, preventing coalescence upon annealing. However, Co NPs conserve their gas-phase structure when deposited by soft landing on the substrate, and therefore, no significant strain is expected due to the attachment on the support. We have recently shown by magnetic measurements of Co NPs embedded in a carbon matrix, that carbon can diffuse into the first atomic layer of cobalt,[42] while upon annealing at 750 K this mixed C−Co phase is decomposed back to fcc Co and graphitic-like carbon [unpublished data]. Based on the results presented here the formation of extended bulk-like cobalt carbide can be safely excluded, since Co−C formation would cause an observable shift of the Co 2p peak close to the metallic Co BEs.[43] However limited amount of atomic carbon on the surface or subsurface of Co NPs, not detectable in the Co 2p spectrum, is quite likely. Surface adsorbed carbon blocks the reactive sites[8] and it would have decreased the reactivity by preventing initial oxidation of our metallic Co NPs, which was not observed. On the contrary, traces of diluted subsurface carbon might affect significantly the local electronic structure of cobalt by inducing strain and stabilizing metastable surface structures (in our case the w-CoO structure), in a similar way as it has been previously found for subsurface oxygen diluted on Cu, Pd, and Ru.[44] Formation of subsurface carbon is supported also by theoretical calculations showing that carbon adsorbed on cobalt surfaces can easily go subsurface, especially in the presence of coadsorbed oxygen.[45] Consequently, the influence of subsurface carbon species is an attractive scenario to explain the formation of w-CoO on the NPs.

Whichever is the reason for the formation of w-CoO in Co NPs, it is evident from our experimental results that the existence of w-CoO is crucial for the redox behavior of Co NPs. Metallic Co NPs were rapidly oxidized after limited exposure in air at room temperature, while spinel-type Co_3O_4, when formed on NPs (570 K, 0.2 mbar O_2), could be readily removed after annealing at 470 K in H_2 (see Supporting Information S5). Of course, the w-CoO/r-CoO mixture could be further oxidized or reduced, but higher temperatures than those used for the bulk Co crystal were required. Apparently, the w-CoO/r-CoO mixture has proved to be the phase the most difficult to be transformed. As has been shown previously for ~20 nm particles, the w-CoO should be converted to r-CoO before total oxidation to Co_3O_4 can take place.[12] In the same way, reduction of Co_3O_4 to Co is processing in two steps *via* r-CoO formation as an intermediate.[20,21] This has been explained by the large crystallographic restructuring needed to transform w-CoO to Co_3O_4 or Co metal,

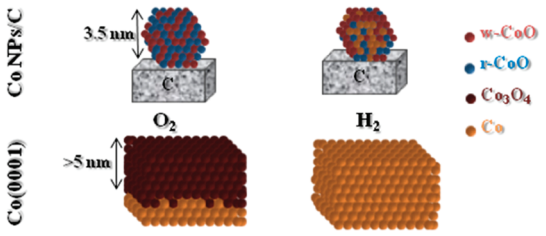

Figure 5. Schematic model illustration of the proposed oxidation state for 3.5 nm Co NPs and Co(0001) crystal in oxidative and reductive environments at 520 K.

while on r-CoO epitaxial growth of Co_3O_4 can directly take place,[12] therefore no restructuring is needed. Besides, recent studies showed that w-CoO is preferentially formed on the surface of r-CoO, epitaxially grown on Ir (100) under UHV conditions.[14,15] Assuming a similar core−shell structure of our oxidized Co NPs with r-CoO in a core and w-CoO as the shell, we can speculate that NPs reduction initiates from the r-CoO core, which is easier to reduce. This picture can explain the decrease in intensity of the Co L_3-edge component at 777 eV, observed at the remaining oxide species after reduction (see Supporting Information S2b), which reflects mainly the preferential reduction of r-CoO. The formation of metallic Co core in reduction conditions suggested by the depth profile results (see Supporting Information S3) can be rationalized by this picture. Similarly, further oxidation to Co_3O_4, seems to be obstructed by the existence of w-CoO in the outermost layers of the NPs. On the basis of the above discussion an illustration model of the extended and nanosized cobalt in reductive and oxidative environments is given in Figure 5.

The results discussed above underlined the differences in the redox behavior of nanosized and extended cobalt. This information is crucial to rationalize the performance of nanosized cobalt in a broad range of applications. For example, it has been found that strain, imposed by the supporting substrate, dramatically influences the magnetic properties of low dimensional CoO films.[2] We showed that several oxide phases, including the metastable w-CoO, can coexist in cobalt NPs, while they are not stable in bulk cobalt under similar conditions. This can produce significant strain in the nanoparticles due to the different lattice parameters of the different oxides. Identification of different oxide phases in nanoparticles, provides the basis to understand, and opens ways to control, the magnetic properties of cobalt. The present finding should be also applicable in catalysis, where the irreducibility of nanocobalt oxides has been traditionally attributed to the formation of mixed oxides with the support.[4] Our work showed another possible origin of this effect, related to nontrivial high kinetic barriers of structural changes in nanosized particles.

METHODS

Preparation of Co NPs. Cobalt nanoparticles (Co NPs) were prepared following the low energy cluster beam deposition technique (LECBD).[42,46] Briefly, Co NPs are vaporized from a Co target using a combined Nd:YAG laser−He gas condensation source. The apparatus is equipped with a quadrupolar electrostatic mass deviator, allowing mass-selection of clusters before deposition onto a Si substrate covered by a 10 nm thick amorphous carbon layer in ultra-high-vacuum conditions.[47,48] The size-distribution of Co clusters follows a Gaussian shape with a median diameter $Dm = 3.50 \pm 0.22$ nm (~8% with mean size of 4.5 nm corresponds to Co dimers) as derived from TEM measurements (Figure 1a). In previous work it has been shown that the Co-cluster shape is a perfect truncated octahedron in the fcc structure.[49] After preparation, the samples were stored in inert atmosphere and then briefly exposed to air upon transferring to the spectrometer.

Preparation of Co (0001) Crystal. The Co(0001) single crystal was cleaned by standard sputter/annealing cycles in a separate UHV chamber and then transferred to the APPES reaction cell where it was pretreated by oxidation (0.2 mbar O_2 at 520 K) and reduction (0.2 mbar H_2 at 520 K) cycles, until all residual surface carbon disappeared.

APPES and XAS Measurements. *In situ* X-ray photoelectron and absorption spectroscopies (XPS and XAS, respectively) were performed at ISISS beamline at BESSY synchrotron facility at the Helmholtz Zentrum Berlin, in a setup described elsewhere.[44,50] The soft X-ray absorption spectra of the Co $L_{3,2}$ edges were recorded in the Total Electron Yield (TEY) mode, enhanced by additional electrons created by ionization of the gas phase above the sample. The samples were placed on a sample holder, which could be heated from the rear by an IR laser (*cw*, 808 nm). The temperature was measured by a K-type thermocouple fixed onto the sample surface. The gas flow into the analysis chamber was controlled *via* calibrated mass flow controllers. A differentially pumped quadrupole mass spectrometer (QMS) was connected through a leak valve to the experimental cell and the gas phase composition was simultaneously monitored, by *online* mass spectrometry, to the spectroscopic characterization of the surface. The photoelectron spectra were normalized by the storage ring current and the energy dependent incident photon flux, which was measured prior to the measurements using a gold foil with known quantum efficiency. The photon flux obtained has been corrected for higher diffraction orders that contribute only to the background but not to the peak intensity in XPS. The binding energy (BE) scale was calibrated with respect to the Fermi level of the electron analyzer. Quantitative calculations were performed using normalized Co 2p, O 1s, C 1s intensities, taking into account the photon-energy dependence of the atomic subshell photoionization cross sections.[51]

CTM Simulation of the XAS Spectra. The $L_{2,3}$-edges absorption spectra were theoretically simulated using the so-called charge-transfer multiplet (CTM) approach.[52,53] The calculations have been carried out using the CTM4XAS version 3.1 program[54] and literature values for the difference between the core hole potential and the 3d-3d repulsion energy U_{dd}, as well as for the hopping parameters.[26] The L_3 to L_2 ratio in the experimental and theoretical curves is practically the same, therefore for clarity only the L_3 edge is presented.

Acknowledgment. We acknowledge useful discussions with E. Savinova and V. Pierron-Bohnes. Financial support from FP7-FCH-JU-2008-1-CP: ROBANODE, DEMMEA and IRAFC projects is gratefully acknowledged. In addition S.Z. and T.D. would like to thank the BESSY II EUSA program for financial support during the experiments conducted at BESSY. Part of this work has been funded by the French ANR/PNANO-07 (ETNAA) project. The authors would like to thank the BESSY II staff for their help in carrying out the experiments, in particular Rolf Follath for

implementation of the continuous monochromator driving mode for XAS measurements.

Supporting Information Available: Co L-edge XAS spectra and Co 2p photoelectron spectra of Co NPs and Co(0001) crystal at various temperature and gas exposure conditions. This material is available free of charge *via* the Internet at http://pubs.acs.org.

REFERENCES AND NOTES

1. Skumryev, V.; Stoyanov, S.; Zhang, Y.; Hadjipanayis, G.; Givord, D.; Nogues, J. Beating The Superparamagnetic Limit With Exchange Bias. *Nature* **2003,** *423*, 850–853.
2. Csiszar, S. I.; Haverkort, M. W.; Hu, Z.; Tanaka, A.; Hsieh, H. H.; Lin, H.-J.; Chen, C. T.; Hibma, T.; Tjeng, L. H. Controlling Orbital Moment and Spin Orientation in CoO Layers by Strain. *Phys. Rev. Lett.* **2005,** *95*, 187205.
3. Poizot, P.; Laruelle, S.; Grugeon, S.; Dupont, L.; Tarascon, J.-M. Nano-Sized Transition-Metaloxides as Negative-Electrode Materials for Lithium-Ion Batteries. *Nature* **2000,** *407*, 496–499.
4. Khodakov, A. Y.; Chu, W.; Fongarland, P. Advances In the Development of Novel Cobalt Fischer−Tropsch Catalysts for Synthesis of Long-Chain Hydrocarbons and Clean Fuels. *Chem. Rev.* **2007,** *107*, 1692–1744.
5. Iglesia, E. Design, Synthesis, and Use of Cobalt-Based Fischer−Tropsch Synthesis Catalysts. *Appl. Catal. A: Gen.* **1997,** *161*, 59–78.
6. Herranz, T.; Deng, X. Y.; Cabot, A.; Guo, J. G.; Salmeron, M. Influence of the Cobalt Particle Size in the CO Hydrogenation Reaction Studied by *in Situ* X-ray Absorption Spectroscopy. *J. Phys. Chem. B* **2009,** *113*, 10721–10727.
7. Bezemer, G. L.; Bitter, J. H.; Kuipers, H. P. C. E.; Oosterbeek, H.; Holewijn, J. E.; Xu, X. D.; Kapteijn, F.; van Dillen, A. J.; de Jong, K. P. Cobalt Particle Size Effects in the Fischer−Tropsch Reaction Studied with Carbon Nanofiber Supported Catalysts. *J. Am. Chem. Soc.* **2006,** *128*, 3956–3964.
8. den Breejen, J. P.; Radstake, P. B.; Bezemer, G. L.; Bitter, J. H.; Fröseth, V.; Holmen, A.; de Jong, K. P. On the Origin of the Cobalt Particle Size Effects in Fischer−Tropsch Catalysis. *J. Am. Chem. Soc.* **2009,** *131*, 7197–7203.
9. den Breejen, J. P.; Sietsma, J. R. A.; Friedrich, H.; Bitter, J. H.; de Jong, K. P. Design of Supported Cobalt Catalysts with Maximum Activity for the Fischer−Tropsch Synthesis. *J. Catal.* **2010,** *270*, 146–152.
10. Seo, W. S.; Shim, J. H.; Oh, S. J.; Lee, E. K.; Hur, N. H.; Park, J. T. Phase- and Size-Controlled Synthesis of Hexagonal and Cubic CoO Nanocrystals. *J. Am. Chem. Soc.* **2005,** *127*, 6188–6189.
11. Risbud, A. S.; Snedeker, L. P.; Elcombe, M. M.; Cheetham, A. K.; Seshadri, R. Wurtzite CoO. *Chem. Mater.* **2005,** *17*, 834–838.
12. Nam, K. M.; Shim, J. H.; Han, D. W.; Kwon, H. S.; Kang, Y. M.; Li, Y.; Song, H; Seo, W. S.; Park, J. T. Syntheses and Characterization of Wurtzite CoO, Rocksalt CoO, and Spinel Co_3O_4 Nanocrystals: Their Interconversion and Tuning of Phase and Morphology. *Chem. Mater.* **2010,** *22*, 4446–4454.
13. Venkatesan, M.; Fitzgerald, C. B.; Lunney, J. G.; Coey, J. M. D. Anisotropic Ferromagnetism in Substituted Zinc Oxide. *Phys. Rev. Lett.* **2004,** *93*, 177206.
14. Meyer, W.; Hock, D.; Biedermann, K.; Gubo, M.; Müller, S.; Hammer, L.; Heinz, K. Coexistence of Rocksalt and Wurtzite Structure in Nanosized CoO Films. *Phys. Rev. Lett.* **2008,** *101*, 016103.
15. Meyer, W.; Biedermann, K.; Gubo, M.; Hammer, L.; Heinz, K. Superstructure in the Termination of CoO(111) Surfaces: Low-Energy Electron Diffraction and Scanning Tunneling Microscopy. *Phys. Rev. B* **2009,** *79*, 121403.
16. Brundle, C. R.; Chuang, T. J.; Rice, D. W. X-ray Photoemission Study of Interaction of Oxygen and Air with Clean Cobalt Surfaces. *Surf. Sci.* **1976,** *60*, 286–300.
17. Bridge, M. E.; Lambert, R. M. Oxygen−Chemisorption, Surface Oxidation, and the Oxidation of Carbon Monoxide on Cobalt (0001). *Surf. Sci.* **1979,** *82*, 413–424.
18. Castro, G. R.; Küppers, J. Interaction of Oxygen with hcp (0001) Recrystallized Cobalt Surfaces. *Surf. Sci.* **1982,** *123*, 456–470.
19. Wang, N. L.; Kaiser, U.; Ganschow, O.; Wiedmann, L.; Benninghoven, A. Oxidation of Cobalt at Room-Temperature, Studied by Combined Static SIMS, Static AES, XPS, and Work Function Investigations. *Surf. Sci.* **1983,** *124*, 51–67.
20. Potoczna-Petru, D.; Kepinski, L. Reduction Study of Co_3O_4 Model Catalyst by Electron Microscopy. *Catal. Lett.* **2001,** *73*, 41–46 and refs therein.
21. Bulavchenko, O. A.; Cherepanova, S. V.; Malakhov, V. V.; Dovlitova, L. S.; Ishchenko, A. V.; Tsybulya, S. V. *In Situ* XRD Study of Nanocrystalline Cobalt Oxide Reduction. *Kinet. Catal.* **2009,** *50*, 192–198 and refs therein.
22. Martin, M.; Koops, U.; Lakshmi, N. Reactivity of Solids Studied by *in Situ* XAS and XRD. *Solid State Ionics* **2004,** *172*, 357–363 and references therein.
23. Palasantzas, G.; Vystavel, T.; Koch, S. A.; de Hosson, J. T. M. Coalescence Aspects of Cobalt Nanoparticles During *in Situ* High-Temperature Annealing. *J. Appl. Phys.* **2006,** *99*, 024307.
24. Petitto, S. C.; Marsh, E. M.; Carson, G. A.; Langell, M. A. Cobalt Oxide Surface Chemistry: The Interaction of CoO(100), Co_3O_4(110), and Co_3O_4(111) with Oxygen and Water. *J. Mol. Catal. A* **2008,** *281*, 49–58.
25. Bazin, D.; Kovács, I.; Guczi, L.; Parent, P.; Laffon, C.; de Groot, F.; Ducreux, O.; Lynch, J. Genesis of Co/SiO_2 Catalysts: XAS Study at the Cobalt L-III,L-II Absorption Edges. *J. Catal.* **2000,** *189*, 456–462.
26. Morales, F.; de Groot, F. M. F.; Glatzel, P.; Kleimenov, E.; Bluhm, H.; Hävecker, M.; Knop-Gericke, A.; Weckhuysen, B. M. *In Situ* X-ray Absorption of $Co/Mn/TiO_2$ Catalysts For Fischer−Tropsch Synthesis. *J. Phys. Chem. B* **2004,** *108*, 16201–16207.
27. Vaz, C. A. F.; Prabhakaran, D.; Altman, E. I.; Henrich, V. E. Experimental Study of the Interfacial Cobalt Oxide in Co_3O_4/α-Al_2O_3(0001) Epitaxial Films. *Phys. Rev. B* **2009,** *80*, 155457.
28. Petitto, S. C.; Langell, M. A. Surface Composition and Structure of Co_3O_4(110) and the Effect of Impurity Segregation. *J. Vac. Sci. Technol. A* **2004,** *22*, 1690–1696.
29. Nakamura, I.; Haneda, M.; Hamada, H.; Fujitani, T. Direct Decomposition of Nitrogen Monoxide Over a K-Deposited Co(0001) Surface: Comparison to K-Doped Cobalt Oxide Catalysts. *J. Electron Spectrosc. Relat. Phenom.* **2006,** *150*, 150–154.
30. Zafeiratos, S.; Dintzer, T.; Teschner, D.; Blume, R.; Hävecker, M.; Knop-Gericke, A.; Schlögl, R. Methanol Oxidation over Model Cobalt Catalysts: Influence of the Cobalt Oxidation State on the Reactivity. *J. Catal.* **2010,** *269*, 309–317.
31. Jaffari, G. H.; Lin, H.-Y.; Ni, C.; Shah, S. I. Physiochemical Phase Transformations in Co/CoO Nanoparticles Prepared by Inert Gas Condensation. *Mater. Sci. Eng. B* **2009,** *164*, 23–29.
32. Boyen, H.-G.; Kästle, G.; Zürn, K.; Herzog, T.; Weigl, F.; Ziemann, P.; Mayer, O.; Jerome, C.; Möller, M.; Spatz, J. P.; *et al*. Micellar Route to Ordered Arrays of Magnetic Nanoparticles: From Size-Selected Pure Cobalt Dots to Cobalt-Cobalt Oxide Core-Shell Systems. *Adv. Funct. Mater.* **2003,** *13*, 359–364.
33. Khodakov, A. Yu.; Lynch, J.; Basin, D.; Rebours, B.; Zanier, N.; Moisson, B.; Chaumette, P. Reducibility of Cobalt Species in Silica-Supported Fischer−Tropsch Catalysts. *J. Catal.* **1997,** *168*, 16–25.
34. NPs spectra were recorded in O_2 while for Co(0001) a mixture of O_2/H_2 was used. The peaks are normalized in height and shifted at the same BE so as differences in the satellite structure to be pronounced.
35. Escax, V.; Champion, G.; Arrio, M.-A.; Zacchigna, M.; dit Moulin, C. C.; Bleuzen, A. The Co Ligand Field: A Key Parameter in Photomagnetic CoFe Prussian Blue Derivatives. *Angew. Chem.* **2005,** *44*, 4798–4801.
36. dit Moulin, C. C.; Champion, G.; Cafun, J. −D.; Arrio, M.-A.; Bleuzen, A. Structural Rearrangements Induced by Photoexcitation in a RbCoFe Prussian Blue Derivative. *Angew. Chem.* **2007,** *46*, 1287–1289.

37. Kumagai, Y.; Ikeno, H.; Oba, F.; Matsunaga, K.; Tanaka, I. Effects of Crystal Structure on Co-L-2,L-3 X-ray Absorption Near-Edge Structure and Electron-Energy-Loss Near-Edge Structure of Trivalent Cobalt Oxides. *Phys. Rev. B* **2008,** *77*, 155124.
38. García-Fernández, P.; García-Lastra, J. M.; Aramburu, J. A.; Barriuso, M. T.; Moreno, M. Strong Dependence of 10*Dq* on the Metal-Ligand Distance: Key Role Played by the s−p Hybridization on Ligands. *Chem. Phys. Lett.* **2006,** *426*, 91–95.
39. Meyerheim, H. L.; Tusche, C.; Ernst, A.; Ostanin, S.; Maznichenko, I. V.; Mohseni, K.; Jedrecy, N.; Zegenhagen, J.; Roy, J.; Mertig, I.; Kirschner, J. Wurtzite-Type CoO Nanocrystals in Ultrathin ZnCoO Films. *Phys. Rev. Lett.* **2009,** *102*, 156102.
40. Netze, F. P.; Allegretti, F.; Surnev, S. Low-Dimensional Oxide Nanostructures on Metals: Hybrid Systems with Novel Properties. *J. Vac. Sci. Technol. B* **2010,** *28*, 1–16.
41. Sprouster, D. J.; Giulian, R.; Araujo, L. L.; Kluth, P.; Johannessen, B.; Cookson, D. J.; Foran, G. J.; Ridgway, M. C. Structural and Vibrational Properties of Co Nanoparticles Formed by Ion Implantation. *J. Appl. Phys.* **2010,** *107*, 014313.
42. Tamion, A.; Raufast, C.; Hillenkamp, M.; Bonet, E.; Jouanguy, J.; Canut, B.; Bernstein, E.; Boisron, O.; Wernsdorfer, W.; Dupuis, V. Magnetic Anisotropy of Embedded Co Nanoparticles: Influence of the Surrounding Matrix. *Phys. Rev. B* **2010,** *81*, 144403.
43. Poon, S. W.; Pan, J. S.; Tok, E. S. Nucleation and Growth of Cobalt Nanostructures on Highly Oriented Pyrolytic Graphite. *Phys. Chem. Chem. Phys.* **2006,** *8*, 3326–3334.
44. Salmeron, M.; Schögl, R. Ambient Pressure Photoelectron Spectroscopy: A New Tool for Surface Science and Nanotechnology. *Surf. Sci. Rep.* **2008,** *63*, 169–199 and refs therein.
45. Zonnevylle, M. C.; Geerlings, J. J. C.; van Santen, R. A. Conversion of Surface Carbidic to Subsurface Carbon on Cobalt (0001)—A Theoretical Study. *Surf. Sci.* **1990,** *240*, 253–262.
46. Perez, A.; Dupuis, V.; Tuaillon-Combes, J.; Bardotti, L.; Prevel, B.; Bernstein, E.; Mélinon, P.; Favre, L.; Hannour, A.; Jamet, M. Functionalized Cluster-Assembled Magnetic Nanostructures For Applications to High Integration-Density Devices. *Adv. Eng. Mater.* **2005,** *7*, 475–485.
47. Tainoff, D.; Bardotti, L.; Tournus, F.; Guiraud, G.; Boisron, O.; Mélinon, P. Self-Organization of Size-Selected Bare Platinum Nanoclusters: Toward Ultradense Catalytic Systems. *J. Phys. Chem. C* **2008,** *112*, 6842–6849.
48. Tamion, A.; Raufast, C.; Bonet, E.; Dupuis, V.; Fournier, T.; Crozes, T.; Bernstein, E.; Wernsdorfer, W. Magnetization Reversal of a Single Cobalt Cluster Using a RF Field Pulse. *J. Magn. Magn. Mater.* **2010,** *622*, 1315–1318.
49. Jamet, M.; Wernsdorfer, W.; Thirion, C.; Mailly, D.; Dupuis, V.; Mélinon, P.; Pérez, A. Magnetic Anisotropy of a Single Cobalt Nanocluster. *Phys. Rev. Lett.* **2001,** *86*, 4676–4679.
50. Knop-Gericke, A.; Kleimenov, E. V.; Havecker, M.; Blume, R.; Teschner, D.; Zafeiratos, S.; Schlögl, R.; Bukhtiyarov, V. I.; Kaichev, V. V.; Prosvirin, I. P.; *et al.* X-ray Photoelectron Spectroscopy for Investigation of Heterogeneous Catalytic Processes. *Adv. Catal.* **2009,** *52*, 213–272.
51. Yeh, J. J.; Lindau, I. Atomic Subshell Photoionization Cross-Sections and Asymmetry Parameters—1 Less-Than-or-Equal-to *Z* Less-Than-or-Equal-to 103. *At. Data Nucl. Data Tables* **1985,** *32*, 1–155.
52. de Groot, F. High Resolution X-ray Emission and X-ray Absorption Spectroscopy. *Chem. Rev.* **2001,** *101*, 1779–1808.
53. Ikeno, H.; de Groot, F.; Stavitski, E.; Tanaka, I. Multiplet Calculations of L-2,L-3 X-Ray Absorption Near-Edge Structures for 3d Transition-Metal Compounds. *J. Phys.: Condens. Matter.* **2009,** *21*, 104208.
54. Stavitski, E.; de Groot, F. M. F. The CTM4XAS Program for EELS and XAS Spectral Shape Analysis of Transition Metal L Edges. *Micron* **2010,** *41*, 687–694.